LIMNOLOGY AND OCEANOGRAPHY
Letters

ASLO
Open Access

Limnology and Oceanography Letters 2024

doi: 10.1002/lol2.10387

LETTER

Measurements of the inherent optical properties of aqueous suspensions of microplastics

Daniel Koestner[1]* *Robert Foster*[2] *Ahmed El-Habashi*[2] *Shea Cheatham*[1]

[1]Department of Physics and Technology, University of Bergen, Bergen, Norway; [2]Remote Sensing Division, U.S. Naval Research Laboratory, Washington, DC, USA

Scientific Significance Statement

Plastics are becoming an increasingly abundant source of marine debris throughout the global ocean. Compared to macroplastics, marine microplastics are of particular concern given their relatively high number concentration, small size, and ability to enter the base of marine food webs. Currently, quantification of marine microplastics is limited by manual collection and counting, resulting in an incomplete assessment of global stocks. Optical methods can provide a means to circumnavigate these spatial and temporal limitations for global analyses. We present high-quality and comprehensive measurements of the spectral absorption and angular scattering properties of various microplastic assemblages consisting predominantly of particles less than 150 μm in diameter. These measurements are crucial for the development of optical methods to detect microplastics. We also identify several unique optical characteristics which can inform the development of such techniques.

Abstract

Libraries of inherent optical properties (IOPs) of microplastics are sparse, yet they are essential for the development of optical techniques to detect and quantify microplastics in the ocean. In this study, we describe our results and technique for the measurement of the IOPs of microplastic suspensions generated from commonly utilized plastics. The measurements included angle-resolved polarized light scattering, and spectral absorption and beam attenuation coefficients. We also performed ancillary characterization of particle properties, including size distribution, shape, and mass concentration of suspended matter. We observed several unique optical characteristics regarding absorption, scattering, and polarization properties compared with typical marine particle assemblages. We show that these results are useful for radiative transfer simulations as well as the potential development of novel plastic detection techniques from above- or in-water optical measurements.

*Correspondence: daniel.koestner.optics@gmail.com

Associate editor: Angelicque White

Author Contribution Statement: DK led the manuscript effort and prepared the first draft. All authors contributed to, edited, and approved the final manuscript. RF came up with original research questions and acquired initial funding, while DK, RF, and AE designed and implemented the experimental approach. DK prepared figures and managed all scattering, particulate absorption and suspended mass concentration data, RF managed holographic and microscope images, and AE managed hyperspectral absorption and beam attenuation data. SC prepared all radiative transfer simulations with input from DK.

Data Availability Statement: Data are available in SEANOE (https://doi.org/10.17882/98404).

Additional Supporting Information may be found in the online version of this article.

Plastics are becoming increasingly abundant in the ocean (UNEP, 2016). Oceanic plastic can be differentiated by composition and size, as well as the extent of physical and photodegradation (GESAMP 2019). All forms of oceanic plastic have potential consequences to the marine environment and ultimately human health, not all of which have been identified (Van Cauwenberghe and Janssen 2014; Rist et al. 2018). The size of plastic litter is particularly important for understanding its distribution and impact within marine environments. Macroplastics are typically defined as greater than 2500 μm in diameter while microplastics are less than 1000 μm, although this distinction has not been uniformly adopted (Frias and Nash 2019; Hartmann et al. 2019). Microplastics may be especially concerning, and the largest portion of scientific literature focuses on microplastics near the ocean surface which are larger than about 300 μm; a size-class visible to the naked eye and easily ensnared in typical neuston net tows (e.g., Hidalgo-Ruz et al. 2012; Masura et al. 2015; Setälä et al. 2016; Tamminga et al. 2018; Prata et al. 2019). Particles of these sizes (i.e., > 300 μm) are rarely a significant contributor to bulk optical properties in marine environments (Davies et al. 2014), and these large microplastics are currently thought to be undetectable by some satellite sensors (Hu 2021). To the contrary, optically significant "small" microplastics have not been well-studied (Enders et al. 2015). These smaller microplastics can bioaccumulate at the base of the marine food web (Cole et al. 2013; Brandon et al. 2020; Rogers et al. 2020), are hydrolyzed from larger plastic debris (Gigault et al. 2016; Song et al. 2017), and remain difficult to quantify using neuston net tows and visual identification under microscope (Song et al. 2015). Microplastic fibers are also rarely captured by net tows and represent a significant and underestimated threat to marine ecosystems (Rebelein et al. 2021).

Current methods for quantification of microplastics typically involve time-demanding counting under microscope, sometimes requiring significant sample processing and analyses to help differentiate plastic from particles of natural origin (Masura et al. 2015; Prata et al. 2019; Hildebrandt et al. 2022). Remote detection of positively buoyant macroplastics has strong potential by targeting signals in visible or infrared light (Garaba and Dierssen 2018; Tasseron et al. 2021; Zhou et al. 2021). Recent studies have also found light polarization to be useful for characterizing microplastics in laboratory environments (Yu et al. 2021; Valentino et al. 2022; Li et al. 2023). More studies, especially general feasibility studies, are still needed to develop optical approaches for quantifying small microplastics suspended in seawater. Some important questions remain: are we able to develop optical methods to quantitatively estimate microplastic concentrations, and at what concentrations will remote detection from space or airborne observation systems become feasible? To answer these, measurements of the inherent optical properties (IOPs) of microplastics are needed.

The IOPs of seawater provide a complete description of the interactions of visible light with marine material and are independent of the ambient light field. These include the spectral absorption and scattering properties per unit distance. IOPs are necessary for simulations of the oceanic light field and can facilitate the development of inverse optical algorithms aimed at identifying constituent properties from optical measurements (Gordon et al. 1975; Mobley 1994). Rarely, however, are IOPs of marine particles measured fully; either including spectral scattering with no information on angular distribution (e.g., Barnard et al. 1998) or the complete angle-resolved polarized light scattering properties with minimal additional information (e.g., Voss and Fry 1984). For the above reasons, simulations of radiative transfer in the ocean have relied on assumptions and incomplete measurements of IOPs. In the current study, we describe measurement results of a nearly complete set of IOPs for virgin microplastic suspensions, including spectral absorption and scattering coefficients, and important characteristics of angular scattering. We also present results from initial simulations using these measurements to investigate the possibility of remote detection of marine microplastics with satellite sensors.

Methods

Samples

Industrial-grade sheets of common plastics were utilized as source material for generating suspensions of microplastics (*see* Supporting Information for more details). The five polymer types comprising the sheets were glycol-modified polyethylene terephthalate (PETG), polystyrene (PS), polyvinyl chloride (PVC), polyamide 6 (PA6), and polypropylene (PP). Two additional samples composed of small fibers were also used as source material. The dryer lint (DL) material was generated by collecting lint from a household dryer following a cycle of washing and drying clothing made from synthetic fabrics (primarily polyester, acrylic, and elastane). The polyester fiber (PEF) material contained virgin fiber used for crafting or insulation.

Seawater measurements from two contrasting previous studies with equivalent measurements are used for comparison. San Diego, California (SD) samples were mostly organic- and phytoplankton-dominated, while Prudhoe Bay, Alaska (PB) samples were mostly inorganic- and nonphytoplankton-dominated. More detailed analysis of the samples can be found in Koestner et al. (2018, 2020*a*,*b*, 2021).

Instrumentation

Particle size information was obtained from the LISST-VSF and LISST-HOLO2 (Sequoia Scientific). Inversion of forward-scattering measured by the LISST-VSF is used to derive the number concentration of particles with equivalent spherical diameters $D = 2$–173 μm (Agrawal and Pottsmith 2000). The LISST-HOLO2 instrument collects holographic images to measure the particle number concentration for $D = 10$–5000 μm and resolve particle shape features with approximately 5 μm resolution.

The spectral absorption coefficient of particles $a_p(\lambda)$ was determined using a UV/VIS Lambda 850+ (Perkin Elmer) spectrophotometer equipped with a 15-cm integrating sphere. Measurements were made of particles retained on 25 mm diameter filters (Whatman grade GF/F, nominal pore size 0.7 μm) placed inside the sphere (Stramski et al. 2015; IOCCG Protocol Series 2018). Additional measurements of the spectral absorption $a(\lambda)$ and attenuation $c(\lambda)$ coefficients were made using an ac-s instrument (Seabird Scientific). These data were used to derive the spectral scattering coefficient ($\lambda = 400$–700 nm) of each sample; $b(\lambda) = c(\lambda) - a(\lambda)$.

Angle-resolved polarized light scattering measurements were made with a LISST-VSF instrument. This instrument estimates the volume scattering function β, Mueller matrix elements m_{12} and m_{22}, and the attenuation coefficient at a wavelength of 532 nm. β is then integrated over all or backscattering angles to derive scattering b or backscattering b_b coefficients. More detailed information on the instrument and data processing routines can be found in Koestner et al. (2018, 2020*b*).

Measurement procedure

A concentrated master suspension of each sample was used for diluted measurements of optical properties. Dry mass concentration of suspended particulate matter (SPM) and c (532 nm) for master suspensions were 5–44 g m^{-3} and 1–25 m^{-1}, respectively. Three concentrations were made through the serial addition of master suspension to 1.8 liters of water (deionized, degassed, 0.2 μm filtered) to ensure consistency of the LISST-VSF and ac-s measurements (dilution factors 3–30). For each concentration, 3 sets of 30 measurements (0.2 Hz sample rate) were made with the LISST-VSF using a magnetitic stir bar on low-speed and gentle hand-mixing between measurement sets to support particle suspension. Measurements of the purified water served as a blank for removal during data processing.

All measurement results were dilution corrected and refer to the optical and particulate properties of master suspensions. Only one of the triplicate measurement series was utilized to derive median values reported to avoid uncertainties with low measurement signal or multiple scattering errors, although results were consistent for most samples and prepared concentrations (coefficients of variation <10%). Normalized results are presented for comparisons of microplastic and seawater samples to avoid differences in magnitude associated with concentration.

Results

Shape and size

Microscope images of dehydrated master suspensions are presented in Fig. 1. The effects of sample preparation on various plastic types resulted in a variety of particle shapes and sizes represented. Some plastic types (e.g., PETG and PP) displayed highly irregular shapes with lots of microstructure, while PVC contained dense and less irregular shapes. PS samples displayed discernible folding patterns due to the expansion process during manufacture. In contrast, DL and PEF contained long fibrous particles. DL fibers were coarser and more varied while PEF fibers were smoother and more uniform. Of note, these images have some striking resemblance to detrital material at sea exemplifying challenges for visual identification of microplastics in seawater.

Figure 2 contains a summary of quantitative particle size and shape information. The particle size distributions are Junge-like without any clear populations, confirming that a continuous size-spectrum of particles was generated for each sample. There is variability between samples with PS containing relatively more larger particles ($D > 100$ μm) and PA6 containing the relative fewest mid-sized particles in the 10–20 μm range. Some noticeable differences among the extra DL, PEF, and PS samples can also be observed throughout the size range (Fig. 2a). Although the maximum particle size for samples was 650 μm based on sample preparation, only one sample (PS) contained suspended particles greater than 250 μm based on LISST-HOLO2 observations and 90% of total particle volumes were typically accounted for by particles less than 150 μm in diameter. Median diameters were 18–115 μm with an average value of about 50 μm based on LISST-VSF measurements, while median diameters from LISST-HOLO2 ranged 30–115 μm with an average value of about 58 μm. These size metrics are comparable to observations of small microplastics in the Atlantic Ocean (Enders et al. 2015). We can also assume that particles smaller than 2 μm are contributing to optical properties, although we have no definitive observations in this size range.

Regarding particle shape, eccentricity of particles increases with particle size with the least circular particles found typically greater than 100 μm (Fig. 2b). These measurements also confirm that the two fibrous samples (i.e., DL and PEF) had the highest eccentricity values (often greater than 0.90), although PEF tended to have higher values while DL had a larger range of values; a reasonable finding considering the source material of the DL (Fig. 1). All other samples which were blended had eccentricity values $\sim$ 0.75–0.80.

Absorption

The absorption coefficients of microplastic samples are shown in Fig. 3a. Here, absorption coefficients are normalized by SPM for comparison of absorption properties regardless of particle concentration. Generally, the microplastic samples have absorption spectra reminiscent of non-algal material without strong peaks and increasing absorption with decreasing wavelength of light. The microplastics also display relatively high ultraviolet absorption (Fig. 3a; $\lambda < 400$ nm). The PS sample, which appeared dark gray, has a flat absorption spectrum most likely related to pigmentation added during the manufacturing process. The DL sample also

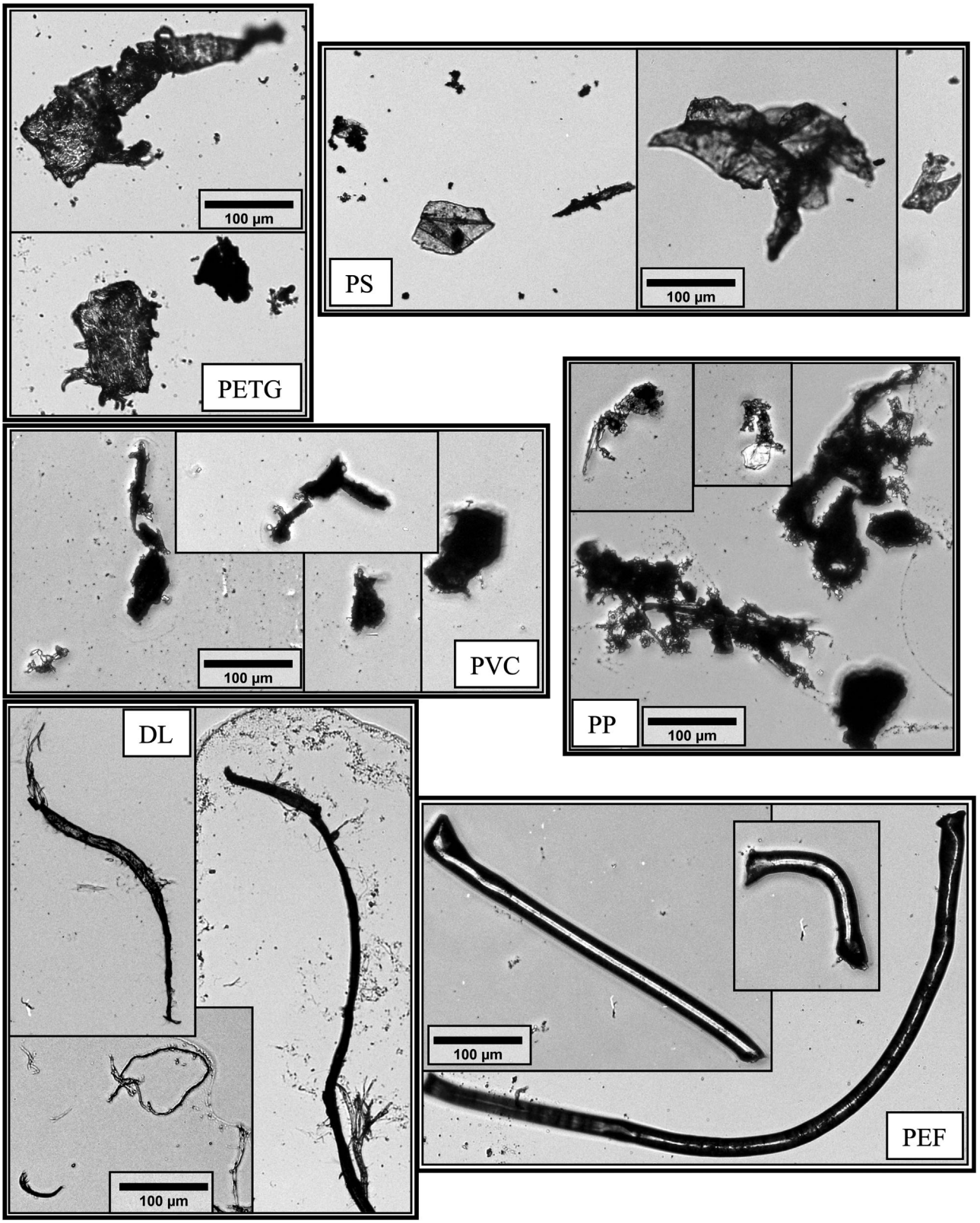

Fig. 1. Microscope images of microplastic samples. Sample IDs are displayed within each set of images. The scale bars shown in boxes apply to all images. No images are shown for PA6. Reproduced from Koestner et al. (2023).

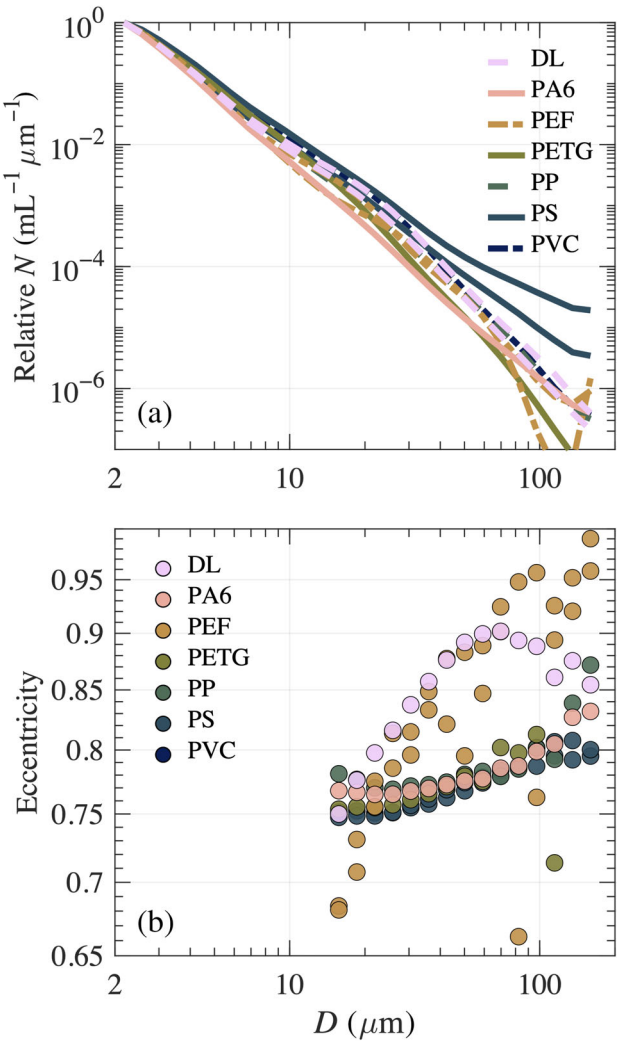

Fig. 2. Particle size and shape information for the microplastic samples. (**a**) Relative number of particles per milliliter normalized by bin-width derived from forward-scattering measurements with LISST-VSF. Power-law exponents are approximately 2.7–3.7. (**b**) Mean eccentricity per size-bin from analysis of measurements with LISST-HOLO2 instrument. Data are plotted as functions of equivalent spherical diameter D. Eccentricity is calculated as $\sqrt{1-(y^2/x^2)}$, where y is minor and x is major axis length of the projected area.

displays some unique absorption features near 600–650 nm owing to the presence of various clothing pigments. Figure 3a also includes a selection of seawater samples from contrasting coastal environments for comparison. Many seawater samples display patterns associated with phytoplankton pigments with absorption peaks in blue and red regions of the spectrum overlayed on a non-algal signal representable by an exponential function. Overall, most microplastic samples had lower absorption per unit mass in the blue portion of light compared with nearly all seawater samples included in this analysis.

Scattering

Angular scattering properties of microplastic and seawater samples are described in Fig. 3b. The particulate phase function $\tilde{\beta}_p$ is a normalized function which describes the angular distribution of unpolarized light scattering with scattering angle $\psi = 0°$ representing initial direction of light propagation. The microplastic $\tilde{\beta}_p$ show a similar pattern to the seawater samples with highly peaked near-forward scattering functions spanning over 4 orders of magnitude from near-forward to backward angles (Fig. 3b). However, unlike most seawater samples, the microplastic samples tend to have higher values of $\tilde{\beta}_p$ for scattering angles approximately 45–180° and backscattering ratios of ~2%–6%. By definition $\tilde{\beta}_p$ integrates to a constant value, and the differences in backwards angles between microplastic and seawater samples are balanced by increased forward scattering signal of seawater samples around 1–10° (not shown). PEF, PVC, and PS samples had distinctly high $\tilde{\beta}_p$ values in the backward angles compared with all seawater samples analyzed.

Polarization

Polarization properties of microplastic and seawater samples are shown in Fig. 3c,d. Here, we present partial results of the 4×4 scattering Mueller matrix m which describes the complete transformation of polarized light and can typically be reduced to six independent elements for randomly oriented natural assemblages of particles (van de Hulst 1957). The degree of linear polarization of light $\mathrm{DoLP_p}$ (defined as $-m_{12}/m_{11}$) describes the proportion of scattered light which is polarized linearly with positive values indicating vertical polarization. Apart from PEF samples, all microplastic samples had relatively low maximum values of $\mathrm{DoLP_p}$ near 90° compared with seawater samples, of which PP and PVC samples had very low maximum values less than about 0.2 (Fig. 3c). These low values indicate that scattered light is more randomly polarized, even at side-scattering angles where seawater samples tend to induce more vertically polarized scattered light. The PS samples appear to have more erratic $\mathrm{DoLP_p}$ functions likely from large particles occasionally entering the laser beam (Fig. 2). Interestingly, PEF samples had $\mathrm{DoLP_p}$ values which are higher than most seawater samples.

The m_{22} matrix element normalized by m_{11} describes cross-polarization effects of linearly polarized light and should be equal to 1 for homogenous spherical particles (van de Hulst 1957). Here, some data are excluded due to uncertainty in measurement reliability over certain angular ranges (Koestner et al. 2020*b*). For scattering angles around 70°, we found that microplastic samples (except for one PEF sample) had lower values of m_{22}/m_{11} compared with most seawater samples. The same is generally seen for backscattering angles around 110°, although the differences between seawater and fibrous samples DL and PEF are less apparent. We note that particle orientation likely effects m_{22}/m_{11}. Whereas SD and microplastic samples were likely well-mixed and randomly

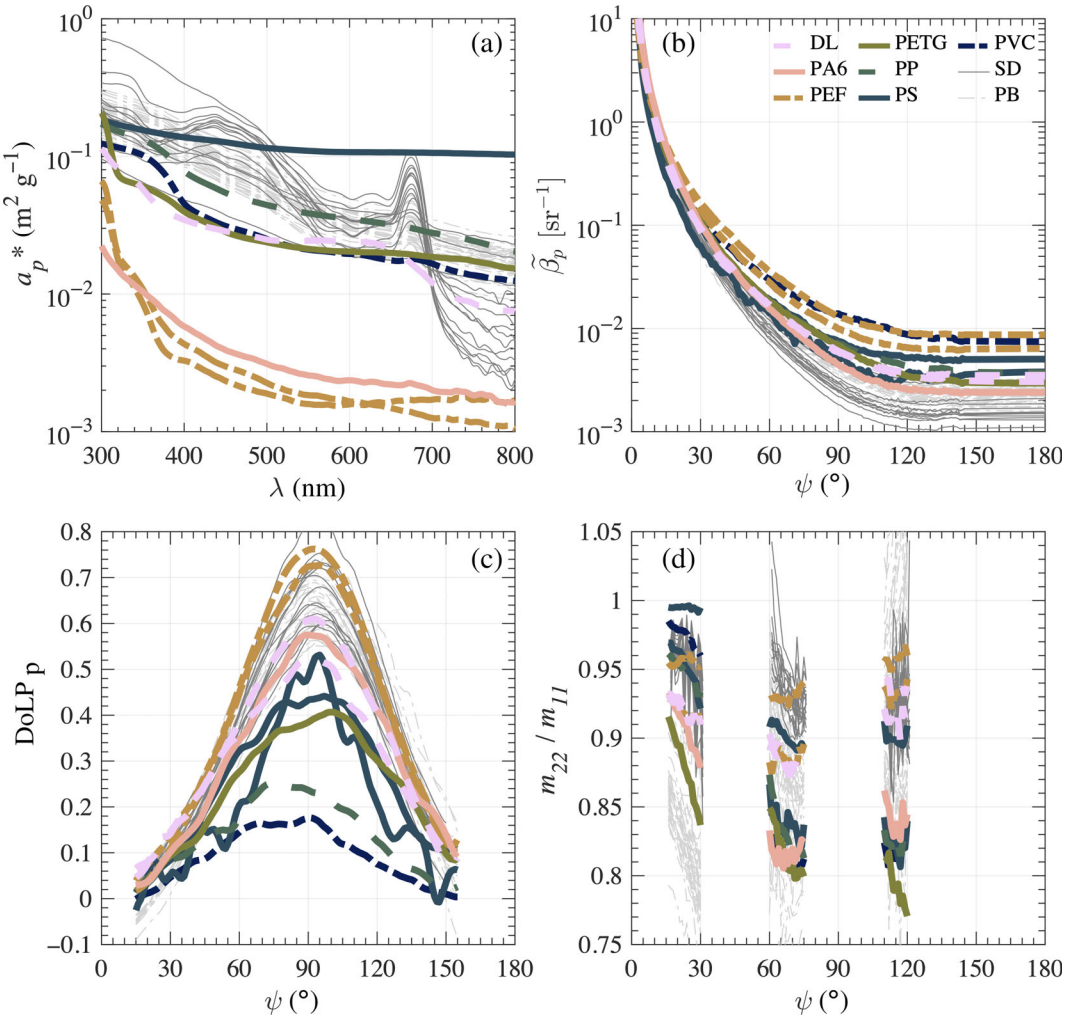

Fig. 3. Absorption and light scattering properties of microplastic and seawater samples. (**a**) Particulate absorption coefficients normalized by mass concentration, (**b**) Phase function, (**c**) Degree of linear polarization, and (**d**) Mueller matrix element m_{22} normalized by m_{11}. Microplastic samples are shown with colored lines while seawater samples from coastal San Diego, California (SD) and near Prudhoe Bay, Alaska (PB) are shown in gray.

oriented during measurements, PB samples were measured in situ with particles likely in preferential orientations.

Discussion

Summary of important optical characteristics

The microplastic samples show distinctive optical characteristics which provide a basis for their detection and differentiation from other particles suspended in seawater. Microplastic samples have low absorption per unit mass concentration while having high backscattering compared with seawater samples (Fig. 3a,b). In Fig. 4a, we present a proxy for remote sensing reflectance of particles. This proxy is foundational to the development of many remote sensing reflectance applications in ocean sciences (e.g., Gordon et al. 1975) and generally describes the proportion of sunlight which will reach an above-water downward looking detector. We find that nearly all microplastic samples display high reflectance compared with the seawater samples, especially in the blue portion of the spectrum (Fig. 4a). The exception is PS which also displayed high absorption from added pigmentation (Fig. 3a). We note that photodegradation of microplastics in the ocean surface is expected to result in loss of pigmentation (Martí et al. 2020). The low absorption and high scattering of microplastic samples is also corroborated by the ratio of $b(\lambda)$ to $c(\lambda)$ derived from the ac-s measurements. This ratio ranged from 75% to 95%, increasing with increasing wavelength with PS having the lowest values (not shown).

Finally, it was found that microplastic samples tend to depolarize light more than typical seawater samples, especially around scattering angles 60–120° (Fig. 3c,d). In Fig. 4b, we present a summary of depolarization characteristics which show that microplastic samples tend to cluster in the lower left portion of the scatterplot indicating scattering which

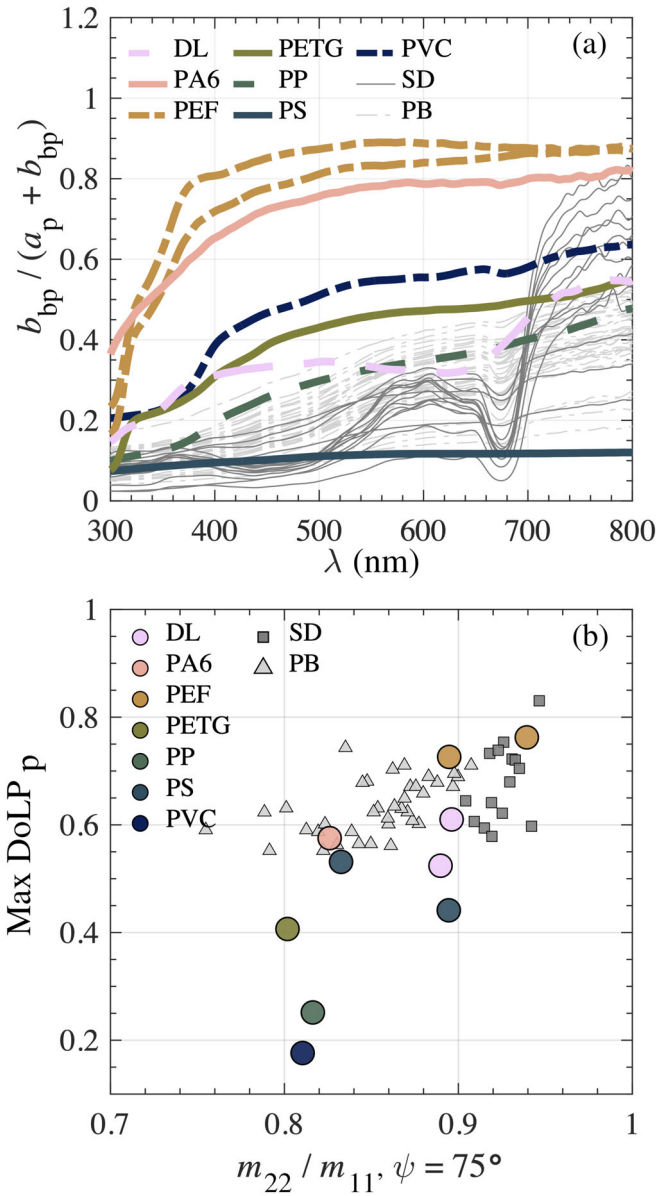

Fig. 4. (**a**) Proxy for particulate reflectance defined as the backscattering coefficient b_{bp} normalized by the sum of the absorption and backscattering coefficients ($a_p + b_{bp}$) for microplastic samples and seawater samples from near Prudhoe Bay, Alaska (PB). (**b**) Scatterplot examining linear depolarization by plotting maximum value of $DoLP_p$ vs. m_{22}/m_{11} at 75° scattering angle for microplastic and seawater samples as indicated.

induces more randomly oriented polarization. The main exception is PEF which scatters light with more linear polarization than most seawater samples. Polarization of light through scattering is complex; however, it can be expected that highly irregular or "rough" particle shapes can strongly depolarize light (Mishchenko et al. 2000). We believe that the highly smooth surfaces of PEF (Fig. 1) may explain lower depolarization (Fig. 4b) and natural weathering processes can roughen the smooth surface of the virgin PEF samples. Nonetheless, most microplastic samples tend to depolarize light more than typical seawater samples (Fig. 4b). Thus, it can be expected that the use of polarizing filters should aid in the identification or quantification of microplastic particles suspended in seawater. Although routine use of polarization in remote optical detection is generally limited to atmospheric material (Hansen and Travis 1974), polarization can be useful in ocean observing (Chami 2007; Loisel et al. 2008; Ibrahim et al. 2016).

Implications to above-water detection of microplastics

Recently, Hu (2021) proposed that the sensitivity of satellite sensors is not sufficient to detect the expected floating areal coverage of microplastics. This analysis relied on surface densities from neuston net trawls and focused on near-infrared bands of the multispectral imager on Sentinel-2. Importantly, the use of longer wavelengths limits detection to mainly floating material as there is minimal depth penetration of near-infrared sunlight. As a follow-up, we utilized our measurements in radiative transfer simulations to determine the suspended mass concentrations of microplastics necessary for remote detection (Stamnes et al. 2018). Here, we examine all visible bands of the Ocean and Land Color Instrument (OLCI) on Sentinel-3, a sensor with higher radiometric sensitivity partially at the expense of lower spatial resolution for measuring bulk optical properties. In Fig. 5, we present simulation results of the remote sensing reflectance from two water bodies representative of the South Pacific Subtropical Gyre with varying concentrations of microplastics. The addition of microplastics increases reflected light for nearly all wavelengths (Fig. 5a,b). Assuming an equal-part mixture of PEF, PETG, and PP distributed homogeneously throughout the water column, the detectable SPM for most visible bands of OLCI is about 10 mg m^{-3}, with concentrations as low as 2 mg m^{-3} detectable with blue and green bands (Fig. 5c,d). Importantly, this represents a potential minimum concentration that might be detectable based on our simulations, assumptions, and experimental measurements, and does not guarantee differentiation from other material in seawater. Assuming realistic uncertainty in the background material (i.e., varying the algal and nonalgal contributions; Supporting Information Fig. S3), the limit of around 2 mg m^{-3} is only detectable at 510 nm, while relatively large changes in reflected blue light are seen following changes in background composition (Fig. 5c,d). We refer to estimates of the average surface mass concentration of microplastics in the Great Pacific Garbage Patch as approximately 2.5 kg km^{-2} (or SPM = 33 mg m^{-3} assuming half of the 15-cm Manta trawl was submerged), noting the microplastic size range was 0.5–5 mm and this refers mainly to buoyant material (Lebreton et al. 2018).

Concluding remarks

In this study we present the first, to our knowledge, comprehensive measurement results of the IOPs of common microplastic suspensions. We generated suspensions with continuous size-spectrums ranging from less than 2 μm to over 100 μm in

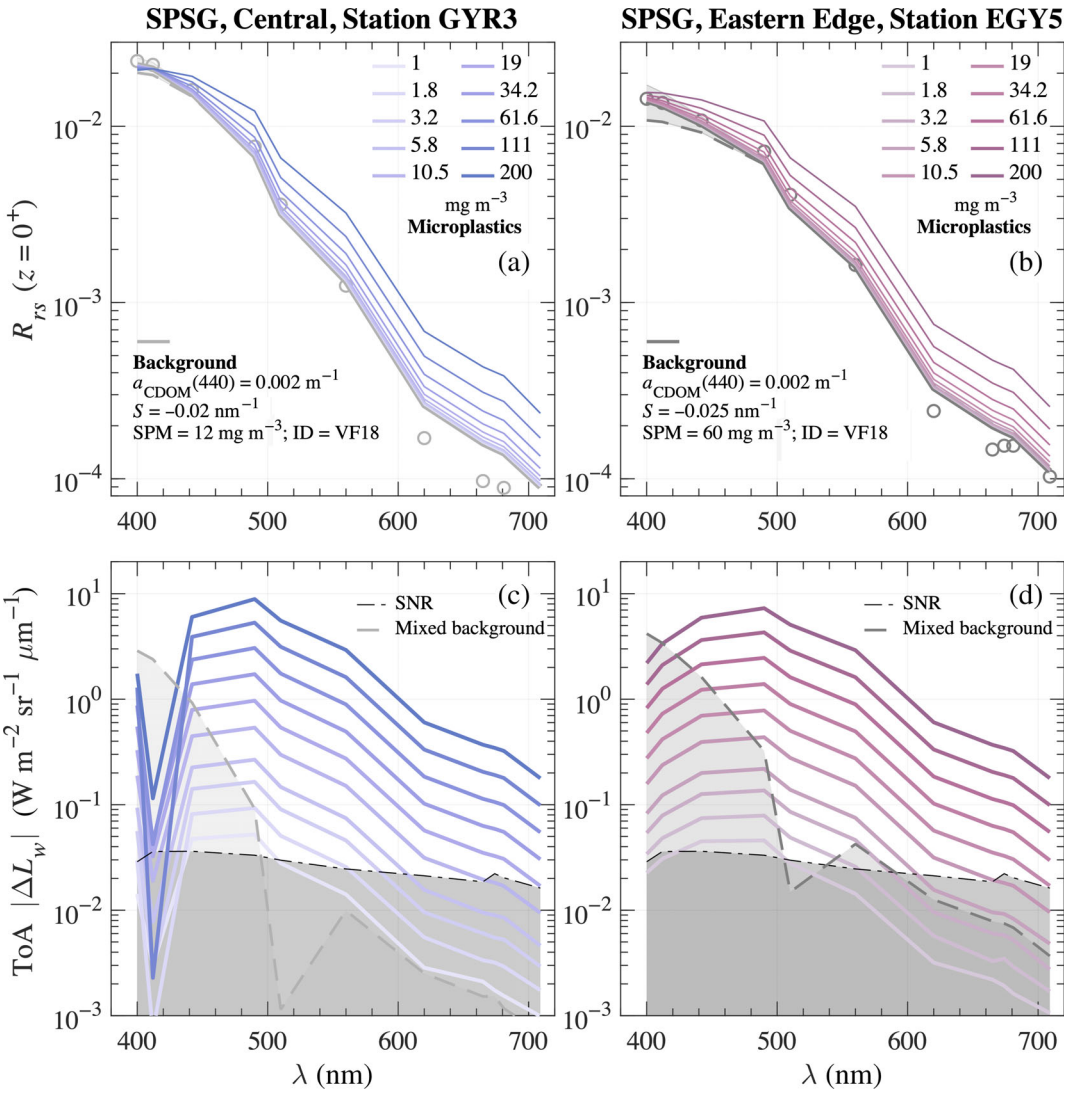

Fig. 5. Summary of radiative transfer simulations for an ocean–atmosphere system at bottom of atmosphere (**a**,**b**) and top of atmosphere (**c**,**d**) for two backgrounds representing center (**a**,**c**) and edge (**b**,**d**) of the South Pacific Subtropical Gyre (SPSG). Results are presented for the background (gray solid lines) with various dry suspended mass concentrations (SPM) of microplastics added (colored solid lines) as indicated in legends. Microplastic concentrations refer to total SPM of an equal-part mixture of PEF, PETG, and PP added to the background. (**a**,**b**) Remote sensing reflectance just above the ocean surface, R_{rs} $(z = 0^+)$. The background composition in terms of SPM of San Diego sample VF18 and absorption coefficient of colored dissolved organic matter (a_{CDOM}) at 440 nm and its exponential slope (S) is shown in the panel. A gray dashed line refers to an alternate background which is composed of an equal-parts mixture of San Diego samples VF17 (nonalgal and organic dominated) and VF18 (algal and organic dominated) describing reasonable variability in background composition. Gray open circles denote measured R_{rs} $(z = 0^+)$ reported in Stramski et al. (2008), generally supporting chosen background optical properties and validity of simulations to approximate the GYR3 and EGY5 stations from the BIOSOPE cruise. (**c**,**d**) absolute difference in upwelling radiance (ΔL_w) from background at the top of atmosphere (ToA). A dash-dotted line and darker shaded area represent the technical specifications of the signal-to-noise ratio (SNR) for Sentinel-3 OLCI (Donlon et al. 2012), while the dashed line and lighter shaded area represent additional uncertainty pertaining to the mixture of background materials. Microplastics can be considered detectable if ΔL_w of added microplastics exceeds both the SNR and the change in signal deriving from varying background composition. See Supporting Information for more details regarding simulations.

diameter with a major contribution of optically significant particles. The spectral absorption and angular scattering properties were measured using state-of-the-art optical instrumentation and with good reproducibility of results. We describe microplastic results in comparison to natural seawater samples from various marine environments. Of most importance, our measurements are more representative of the types of small suspended microplastics that are entering the base of marine food webs (Cole et al. 2013; Brandon et al. 2020) and appear most numerous in oceanic environments (e.g., Song et al. 2014; Enders et al. 2015; Hansen et al. 2023), as opposed to larger microplastics considered in earlier studies (e.g., Garaba and Dierssen 2018; Hu 2021).

With some minor exceptions, we found that microplastics have lower absorption, backscatter more strongly, and depolarize light to a greater extent than natural marine particles. These characteristics may enable optical detection and differentiation from typical material suspended in seawater, especially in open-ocean oligotrophic gyres where many plastics have accumulated (Eriksen et al. 2013; Lebreton et al. 2018). We estimate that microplastic concentrations as low as 2 mg m^{-3} may be detectable by green channels of satellite detectors in these environments, although more dedicated studies are needed to examine effects of vertical distribution of microplastics and the potential for differentiation from natural oceanic material using spectral signatures. We acknowledge that our results are for virgin microplastic suspensions produced in a laboratory environment; however, they represent a pivotal first step. We also urge further studies measuring IOPs of microplastics following biofouling and weathering processes such as photodegradation and natural fragmentation.

References

Agrawal, Y. C., and H. C. Pottsmith. 2000. Instruments for particle size and settling velocity observations in sediment transport. Mar. Geol. **168**: 89–114. doi:10.1016/S0025-3227(00)00044-X

Barnard, A. H., W. S. Pegau, and J. R. V. Zaneveld. 1998. Global relationships of the inherent optical properties of the oceans. J. Geophys. Res. Oceans **103**: 24955–24968. doi:10.1029/98JC01851

Brandon, J. A., A. Freibott, and L. M. Sala. 2020. Patterns of suspended and salp-ingested microplastic debris in the North Pacific investigated with epifluorescence microscopy. Limnol. Oceanogr. Lett. **5**: 46–53. doi:10.1002/lol2.10127

Chami, M. 2007. Importance of the polarization in the retrieval of oceanic constituents from the remote sensing reflectance. J. Geophys. Res. **112**: C05026. doi:10.1029/2006JC003843

Cole, M., P. Lindeque, E. Fileman, C. Halsband, R. Goodhead, J. Moger, and T. S. Galloway. 2013. Microplastic ingestion by zooplankton. Environ. Sci. Tech. **47**: 6646–6655. doi:10.1021/es400663f

Davies, E. J., D. McKee, D. Bowers, G. W. Graham, and W. A. M. Nimmo-Smith. 2014. Optically significant particle sizes in seawater. Appl. Optics **53**: 1067–1074. doi:10.1364/AO.53.001067

Donlon, C., and others. 2012. The global monitoring for environment and security (GMES) sentinel-3 mission. Remote Sens. Environ. **120**: 37–57. doi:10.1016/j.rse.2011.07.024

Enders, K., R. Lenz, C. A. Stedmon, and T. G. Nielsen. 2015. Abundance, size and polymer composition of marine microplastics ≥10 μm in the Atlantic Ocean and their modelled vertical distribution. Mar. Pollut. Bull. **100**: 70–81. doi:10.1016/j.marpolbul.2015.09.027

Eriksen, M., N. Maximenko, M. Thiel, A. Cummins, G. Lattin, S. Wilson, J. Hafner, A. Zellers, and S. Rifman. 2013. Plastic pollution in the South Pacific subtropical gyre. Mar. Pollut. Bull. **68**: 71–76. doi:10.1016/j.marpolbul.2012.12.021

Frias, J. P. G. L., and R. Nash. 2019. Microplastics: Finding a consensus on the definition. Mar. Pollut. Bull. **138**: 145–147. doi:10.1016/j.marpolbul.2018.11.022

Garaba, S. P., and H. M. Dierssen. 2018. An airborne remote sensing case study of synthetic hydrocarbon detection using short wave infrared absorption features identified from marine-harvested macro- and microplastics. Remote Sens. Environ. **205**: 224–235. doi:10.1016/j.rse.2017.11.023

GESAMP. 2019. Guidelines for the monitoring and assessment of plastic litter and microplastics in the ocean, p. 130. *In* P. J. Kershaw, A. Turra, and F. Galgani [eds.], *GESAMP Joint Group of Experts on the Scientific Aspects of Marine Environmental Protection* (GESAMP Reports and Studies, No. 99), London, UK. doi:10.25607/OBP-435

Gigault, J., B. Pedrono, B. Maxit, and A. Ter Halle. 2016. Marine plastic litter: The unanalyzed nano-fraction. Environ. Sci. Nano **3**: 346–350. doi:10.1039/C6EN00008H

Gordon, H. R., O. B. Brown, and M. M. Jacobs. 1975. Computed relationships between the inherent and apparent optical properties of a flat homogeneous ocean. Appl. Opt. **14**: 417–427. doi:10.1364/AO.14.000417

Hansen, J., L. Hildebrandt, T. Zimmermann, F. El Gareb, E. K. Fischer, and D. Pröfrock. 2023. Quantification and characterization of microplastics in surface water samples from the Northeast Atlantic Ocean using laser direct infrared imaging. Mar. Pollut. Bull. **190**: 114880. doi:10.1016/j.marpolbul.2023.114880

Hansen, J. E., and L. D. Travis. 1974. Light scattering in planetary atmospheres. Space Sci. Rev. **16**: 527–610. doi:10.1007/BF00168069

Hartmann, N. B., and others. 2019. Are we speaking the same language? Recommendations for a definition and categorization framework for plastic debris. Environ. Sci. Technol. **53**: 1039–1047. doi:10.1021/acs.est.8b05297

Hidalgo-Ruz, V., L. Gutow, R. C. Thompson, and M. Thiel. 2012. Microplastics in the marine environment: A review of the methods used for identification and quantification. Environ. Sci. Technol. **46**: 3060–3075. doi:10.1021/es2031505

Hildebrandt, L., F. El Gareb, T. Zimmermann, O. Klein, A. Kerstan, K. C. Emeis, and D. Pröfrock. 2022. Spatial distribution of microplastics in the tropical Indian Ocean based on laser direct infrared imaging and microwave-assisted matrix digestion. Environ. Pollut. **307**: 119547. doi:10.1016/j.envpol.2022.119547

Hu, C. 2021. Remote detection of marine debris using satellite observations in the visible and near infrared spectral range: Challenges and potentials. Rem. Sens. Environ. **259**: 112414. doi:10.1016/j.rse.2021.112414

Ibrahim, A., A. Gilerson, J. Chowdhary, and S. Ahmed. 2016. Retrieval of macro- and micro-physical properties of oceanic hydrosols from polarimetric observations. Rem. Sens. Environ. **186**: 548–566. doi:10.1016/j.rse.2016.09.004

IOCCG Protocol Series. 2018. Inherent optical property measurements and protocols: Absorption coefficient. *In* A. R. Neeley and A. Mannino [eds.], *IOCCG Ocean optics and biogeochemistry protocols for satellite ocean colour sensor validation*, v. **1.0**. IOCCG, Dartmouth. doi:10.25607/OBP-119

Koestner, D., R. Foster, and A. El-Habashi. 2023. On the potential for optical detection of microplastics in the ocean. In Frontiers in Ocean Observing: Emerging Technologies for Understanding and Managing a Changing Ocean, p. 49–51. *In* E. S. Kappel, V. Cullen, M. J. Costello, L. Galgani, C. Gordó-Vilaseca, A. Govindarajan, S. Kouhi, C. Lavin, L. McCartin, J. D. Müller, B. Pirenne, T. Tanhua, Q. Zhao, and S. Zhao [eds.], *Oceanography*, v. **36**. doi:10.5670/oceanog.2023.s1.15

Koestner, D., D. Stramski, and R. A. Reynolds. 2018. Measurements of the volume scattering function and the degree of linear polarization of light scattered by contrasting natural assemblages of marine particles. Appl. Sci. **8**: 2690. doi:10.3390/app8122690

Koestner, D., D. Stramski, and R. A. Reynolds. 2020*a*. Assessing the effects of particle size and composition on light scattering through measurements of size-fractionated seawater samples. Limnol. Oceanogr. **65**: 173–190. doi:10.1002/lno.11259

Koestner, D., D. Stramski, and R. A. Reynolds. 2020*b*. Polarized light scattering measurements as a means to characterize particle size and composition of natural assemblages of marine particles. Appl. Optics **59**: 8314–8334. doi:10.1364/AO.396709

Koestner, D., D. Stramski, and R. A. Reynolds. 2021. Characterization of suspended particulate matter in contrasting coastal marine environments with angle-resolved polarized light scattering measurement. Appl. Optics **60**: 11161–11179. doi:10.1364/AO.441226

Lebreton, L., and others. 2018. Evidence that the Great Pacific Garbage Patch is rapidly accumulating plastic. Sci. Rep. **8**: 4666. doi:10.1038/s41598-018-22939-w

Li, J., H. Liu, R. Liao, H. Wang, Y. Chen, J. Xiang, X. Xu, and H. Ma. 2023. Recognition of microplastics suspended in seawater via refractive index by Mueller matrix polarimetry. Mar. Pollut. Bull. **188**: 114706. doi:10.1016/j.marpolbul.2023.114706

Loisel, H., L. Duforet, D. Dessailly, M. Chami, and P. Dubuisson. 2008. Investigation of the variations in the water leaving polarized reflectance from the POLDER satellite data over two biogeochemical contrasted oceanic areas. Opt. Express **16**: 12905–12918. doi:10.1364/OE.16.012905

Martí, E., C. Martin, M. Galli, F. Echevarría, C. M. Duarte, and A. Cózar. 2020. The colors of the ocean plastics. Environ. Sci. Tech. **54**: 6594–6601. doi:10.1021/acs.est.9b06400

Masura, J., J. Baker, G. Foster, and C. Arthur. 2015. Laboratory methods for the analysis of microplastics in the marine environment: Recommendations for quantifying synthetic particles in waters and sediments. https://repository.library.noaa.gov/view/noaa/10296

Mishchenko, M. I., J. W. Hovenier, and L. D. Travis. 2000. *Light scattering by nonspherical particles: Theory, measurements, and applications*. Academic Press.

Mobley, C. D. 1994. *Light and water: Radiative transfer in natural waters*. Academic Press.

Prata, J. C., J. P. da Costa, A. C. Duarte, and T. Rocha-Santos. 2019. Methods for sampling and detection of microplastics in water and sediment: A critical review. Trends Anal. Chem. **110**: 150–159. doi:10.1016/j.trac.2018.10.029

Rebelein, A., I. Int-Veen, U. Kammann, and J. P. Scharsack. 2021. Microplastic fibers—Underestimated threat to aquatic organisms? Sci. Total Environ. **777**: 146045. doi:10.1016/j.scitotenv.2021.146045

Rist, S., B. Carney Almroth, N. B. Hartmann, and T. M. Karlsson. 2018. A critical perspective on early communications concerning human health aspects of microplastics. Sci. Total Environ. **626**: 720–726. doi:10.1016/j.scitotenv.2018.01.092

Rogers, K. L., J. A. Carreres-Calabuig, E. Gorokhova, and N. R. Posth. 2020. Micro-by-micro interactions: How microorganisms influence the fate of marine microplastics. Limnol. Oceanogr. Lett. **5**: 18–36. doi:10.1002/lol2.10136

Setälä, O., K. Magnusson, M. Lehtiniemi, and F. Norén. 2016. Distribution and abundance of surface water microlitter in the Baltic Sea: A comparison of two sampling methods. Mar. Pollut. Bull. **110**: 177–183. doi:10.1016/j.marpolbul.2016.06.065

Song, Y. K., S. H. Hong, M. Jang, G. M. Han, S. W. Jung, and W. J. Shim. 2017. Combined effects of UV exposure duration and mechanical abrasion on microplastic fragmentation by polymer type. Environ. Sci. Tech. **51**: 4368–4376. doi:10.1021/acs.est.6b06155

Song, Y. K., S. H. Hong, M. Jang, G. M. Han, M. Rani, J. Lee, and W. J. Shim. 2015. A comparison of microscopic and spectroscopic identification methods for analysis of microplastics in environmental samples. Mar. Pollut. Bull. **93**: 202–209. doi:10.1016/j.marpolbul.2015.01.015

Song, Y. K., S. H. Hong, M. Jang, J. H. Kang, O. Y. Kwon, G. M. Han, and W. J. Shim. 2014. Large accumulation of

micro-sized synthetic polymer particles in the sea surface microlayer. Environ. Sci. Technol. **48**: 9014–9021. doi:10.1021/es501757s

Stamnes, K., B. Hamre, S. Stamnes, N. Chen, Y. Fan, W. Li, Z. Lin, and J. Stamnes. 2018. Progress in forward-inverse modeling based on radiative transfer tools for coupled atmosphere-snow/ice-ocean systems: A review and description of the AccuRT model. Appl. Sci. **8**: 2682. doi:10.3390/app8122682

Stramski, D., and others. 2008. Relationships between the surface concentration of particulate organic carbon and optical properties in the eastern South Pacific and eastern Atlantic Oceans. Biogeosciences **5**: 171–201. doi:10.5194/bg-5-171-2008

Stramski, D., R. A. Reynolds, S. Kaczmarek, J. Uitz, and G. Zheng. 2015. Correction of pathlength amplification in the filter-pad technique for measurements of particulate absorption coefficient in the visible spectral region. Appl. Optics **54**: 6763–6782. doi:10.1364/AO.54.006763

Tamminga, M., E. Hengstmann, and E. K. Fischer. 2018. Microplastic analysis in the South Funen Archipelago, Baltic Sea, implementing manta trawling and bulk sampling. Mar. Pollut. Bull. **128**: 601–608. doi:10.1016/j.marpolbul.2018.01.066

Tasseron, P., T. Van Emmerik, J. Peller, L. Schreyers, and L. Biermann. 2021. Advancing floating macroplastic detection from space using experimental hyperspectral imagery. Remote Sens. (Basel) **13**: 2335. doi:10.3390/rs13122335

UNEP. (2016). *Marine plastic debris and microplastics: Global lessons and research to inspire action and guide policy change*. United Nations Environment Programme. Available from https://wedocs.unep.org/20.500.11822/7720

Valentino, M., and others. 2022. Intelligent polarization-sensitive holographic flow-cytometer: Towards specificity in classifying natural and microplastic fibers. Sci. Total Environ. **815**: 152708. doi:10.1016/j.scitotenv.2021.152708

Van Cauwenberghe, L., and C. R. Janssen. 2014. Microplastics in bivalves cultured for human consumption. Environ. Pollut. **193**: 65–70. doi:10.1016/j.envpol.2014.06.010

van de Hulst, H. C. 1957. *Light scattering by small particles*. John Wiley and Sons, Inc.

Voss, K. J., and E. S. Fry. 1984. Measurement of the Mueller matrix for ocean water. Appl. Optics **23**: 4427–4439. doi:10.1364/AO.23.004427

Yu, S., J. Dai, R. Liao, L. Chen, W. Zhong, H. Wang, Y. Jiang, J. Li, and H. Ma. 2021. Probing the nanoplastics adsorbed by microalgae in water using polarized light scattering. Optik. **231**: 166407. doi:10.1016/j.ijleo.2021.166407

Zhou, S., T. Kuester, M. Bochow, N. Bohn, M. Brell, and H. Kaufmann. 2021. A knowledge-based, validated classifier for the identification of aliphatic and aromatic plastics by WorldView-3 satellite data. Remote Sens. Environ. **264**: 112598. doi:10.1016/j.rse.2021.112598

Acknowledgments

This research was funded by the US National Aeronautics and Space Administration (80HQTR21T0051) and the Office of Naval Research. This research was initiated while the first author (DK) held an NRC Research Associateship award at the Naval Research Laboratory in Washington, DC and completed with support from European Union's Horizon 2020 research and innovation program under the Marie Skłodowska-Curie grant agreement no. 101034309. We would like to express our gratitude to Shungu Garaba, The Ocean Cleanup, and the European Space Agency for supplying the plastic standard samples and to Dariusz Stramski for loaning the LISST-VSF. Extra special thanks to Børge Hamre for feedback and support while preparing radiative transfer simulations.

Submitted 17 August 2023
Revised 04 February 2024
Accepted 09 March 2024

Supporting information for *Measurements of the inherent optical properties of aqueous suspensions of microplastics*

Daniel Koestner[1*], Robert Foster[2], Ahmed El-Habashi[2], Shea Cheatham[1]

[1]*University of Bergen, Department of Physics and Technology, Bergen, Norway*

[2]*Remote Sensing Division, U.S. Naval Research Laboratory, Washington, District of Columbia, USA*

Microplastic Sample Preparation

To create the microplastic samples, the plastic sheets were grated until 2–4 g of small pieces were collected (Fig. S1). The pieces were then combined in a kitchen blender with approximately 100 ml of water (deionized, 0.2 µm filtered) and 100 g of ice cubes made from the same purified water. The ice cubes prevented melting and aided pulverization of the plastic material. The samples were processed for approximately 5–10 minutes with intermittent manual mixing to generate a size-spectrum of microplastic particles. The DL and PEF samples were cut into smaller fragments using scissors in lieu of blending to preserve their shapes. Finally, all samples were filtered using a ~650 µm mesh to remove large microplastics which would inevitably float or sink out of suspension. Replicate samples of DL, PEF, and PS were prepared to identify sample preparation variability. Images of the master suspensions are shown in Figure S2.

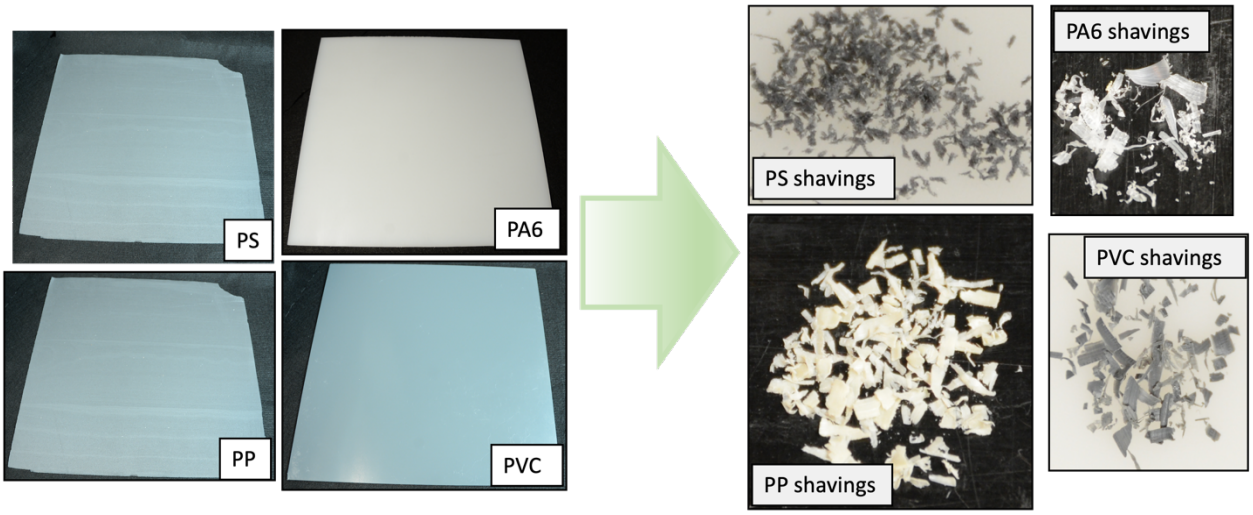

Figure S1. Example images of original plastic sheets (left) and shavings (right) used to generate microplastic master suspensions used in measurements. Plastic IDs: PS = polystyrene; polyamide 6 = PA6; PP = polypropylene; PVC = polyvinyl chloride.

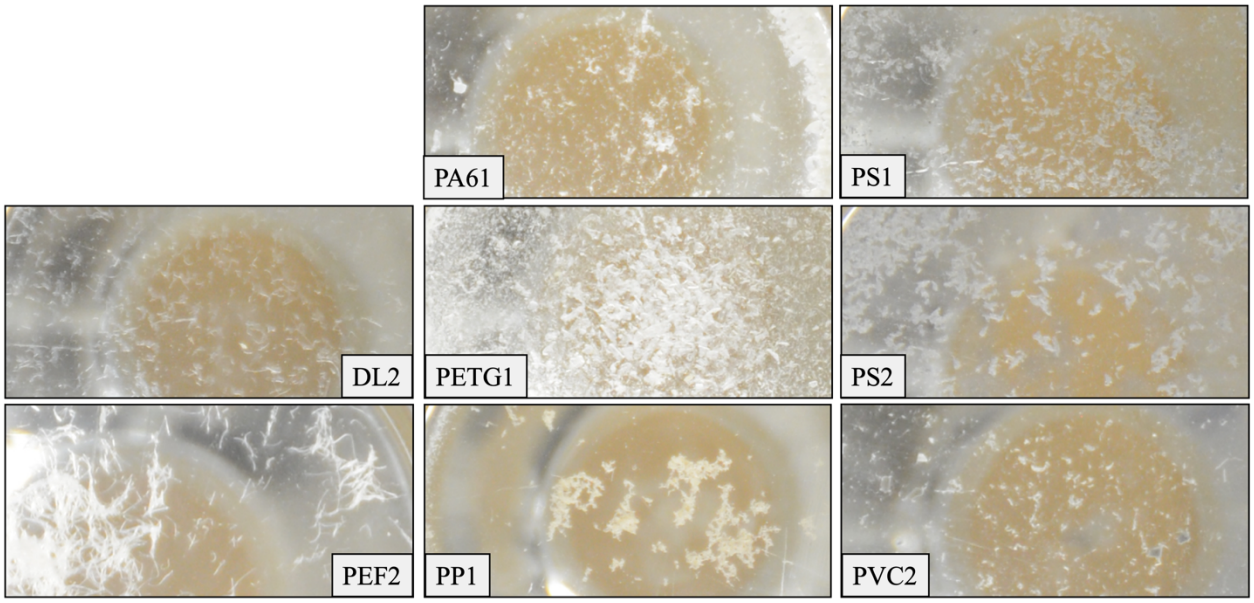

Figure S2. Example images of microplastic master suspensions in 20 mL glass scintillation vials. For reference, the yellow cap shown in each image is approximately 2 cm in diameter. Microplastic IDs: DL = dryer lint; PEF = polyester fibers; polyamide 6 = PA6; PETG = glycol-modified polyethylene terephthalate; PP = polypropylene; PS = polystyrene; PVC = polyvinyl chloride. Note that the number proceeding the microplastic ID in each image refers to the specific sample as some replicates were produced.

Measurement Procedure

A concentrated master suspension of each sample was used as source material for diluted measurements of optical properties. Dry mass concentration of suspended particulate matter (SPM) and c(532 nm) for master suspensions were 5–44 g m^{-3} and 1–25 m^{-1}, respectively. Three concentrations were made through the serial addition of master suspension to 1.8 L of water (deionized, degassed, 0.2 µm filtered) to ensure consistency of the optical measurements (dilution factors 3–30). For each concentration, 3 sets of 30 measurements (0.2 Hz sample rate) were made with the LISST-VSF using a magnetitic stir bar on low-speed and gentle hand-mixing between measurement sets to support particle suspension. A similar procedure was employed for ac-s measurements noting that extra care was taken to minimize air bubble contamination by mounting the instrument at approximately 45º and the influence of settling particles was minimized with a 5 Hz measurement rate.

Measurements of $a_p(\lambda)$ and SPM obtained with 25 mm diameter GF/F filters utilized water from the LISST-VSF measurement chamber.

Undiluted master suspensions were measured in the LISST-HOLO2. Two sets of 200 holograms were collected (2 Hz sample rate) with gentle resuspension of particles using a pipette immediately prior to measurements. Holograms were processed using manufacturer provided software with default settings. The eccentricity and orientation of each particle in each hologram was binned according to its spherical-equivalent diameter, and the mean particle in each size-bin was considered representative.

Radiative Transfer Simulations

Summary

We prepared simulations of remote sensing reflectance R_{rs} (defined as nadir upwelling radiance L_w divided by downwelling irradiance) of a coupled ocean-atmosphere system using solutions to the radiative transfer equation from AccuRT [1] and an input-generating module called Flick [2]. Results were determined for the bottom (10 cm above sea level) and top (12 km above sea level) of a cloud-free aerosol-containing atmosphere. We examined the remote sensing reflectance of an open-ocean background of typical composition with and without microplastics added at all 11 visible bands (400–709 nm) of the ocean and land color instrument (OLCI) on the Sentinel-3 satellite. Efforts were focused on the South Pacific Subtropical Gyre (SPSG), a region of very clear oligotrophic waters which has also been an accumulation zone for plastic debris.

Simulation methods

To simulate the effects of microplastics on the reflectance spectra in the SPSG, we used Flick to generate inherent optical properties as input to AccuRT, a coupled ocean-atmosphere radiative transfer model which solves the radiative transfer equation at any specified depth in a plane-parallel multilayered system. Flick accepts measured IOPs including phase functions as input, and generates parameterized volume scattering functions (i.e., phase function scaled by the scattering coefficient) for input into the model using the delta-fit method [3]. This method finds Legendre polynomial expansion coefficients which minimize the relative least squares residual between the approximate and actual volume scattering functions. The delta-fit method produces highly accurate approximations for most scattering angles while removing some highly forward-peaked scattering, which allow for significantly faster numerical solutions of the radiative transfer equation while realizing the same accuracy. 500 angles (determined with interpolation) were used to sample the volume scattering function for the delta-fit method.

Flick is a shell module which includes user-defined material parameters for easy generation of inputs to AccuRT under various scenarios, including an atmosphere-ocean system. Flick is also a general model for light transport in any specified media and natively includes the measured IOPs of the natural seawater and microplastic samples utilized in the current study. Version 1.0 of Flick was installed and utilized for simulations. It was pulled from github on January 15, 2024 [2].

The simulations output R_{rs}. Note that specularly reflected L_w was subtracted, and 32 streams were used in solving the radiative transfer equation (which is also one less than the number of Legendre polynomial coefficients for the delta-fit of the phase function). 32 streams were used, as this number was found to be more than sufficient for highly accurate results through optimization experiments.

Atmospheric parameters

Solar angle was fixed at 15 degrees from zenith, corresponding with midday summer sun in the SPSG. No clouds were included in any simulations. Atmospheric aerosols were fixed using a total vertical optical thickness of 0.13 at 550 nm, corresponding with typical measurements in the

Pacific Ocean on a clear day [4]. Atmospheric ground temperature was set to 290 K, atmospheric ground pressure to 100 kPa (1 atm), and relative humidity to 50 percent. Atmospheric gas composition was O_3, O_2, H_2O and NO_2 and utilized 8 vertical grid points from atmospheric gas profiles.

Oceanic parameters and background configuration

Water column depth was set to 4000 meters to ensure the removal of sea-bottom effects with a black seafloor. Water salinity and temperature were set to 35 psu and 290 K, respectively. The ocean-atmosphere interface was modeled as a flat Fresnel interface. Simulations were carried out with two backgrounds approximating the spectral reflectance signal obtained from two stations of the South Pacific Subtropical Gyre: GYR3 (center of the gyre) and EGY5 (on the eastern edge of the gyre). These backgrounds are composed of a combination of measured IOPs and estimated absorption coefficient of colored dissolved organic matter (a_{CDOM}) and scattering by air bubbles. Background materials were assumed to be homogenously distributed throughout the entire water column.

The measured IOPs (i.e., spectral mass-specific absorption and scattering coefficients and phase function) used in the background were obtained from the offshore San Diego sample VF18 (also referred to as O_C in [5]) scaled to dry mass concentrations reasonable for the SPSG region (12 and 60 mg m^{-3}) [6]. The a_{CDOM} was estimated using two exponential slopes (–0.02 and –0.025) and a value at 440 nm of 0.002 m^{-1}, which are appropriate for the SPSG [7]. A low concentration of air bubbles (volume fraction of 8.8×10^{-7}) was included as a scattering material with no absorption. The scattering properties of air bubbles were derived from an approximate Mie-code solution for spherical particles with a diameter of 100 μm [8]. These concentrations and absorption values were found to produce simulation results which reasonably match measured R_{rs} in the surface waters of South Pacific Subtropical Gyre (Figure 5). Note that inelastic processes (e.g., Raman scattering) were not included in our simulations and may represent an important source of uncertainty in extremely clear ocean waters [9, 10].

The combined non-water absorption coefficients are shown in Figure S3. Here we also show the absorption coefficient of additional backgrounds computed using an equal-parts mixture of the offshore San Diego samples VF18 and VF17 (also referred to as O_S in [5]). Whereas VF18 (or O_C) represents a particulate assemblage which was algal and organic dominated, VF17 (or O_S) was nonagal and organic dominated and exemplifies some important and reasonable changes to optical properties driven by increased proportions of nonalgal material [5]. These alternate backgrounds were used to examine additional uncertainties in R_{rs} driven by natural variability in optical properties.

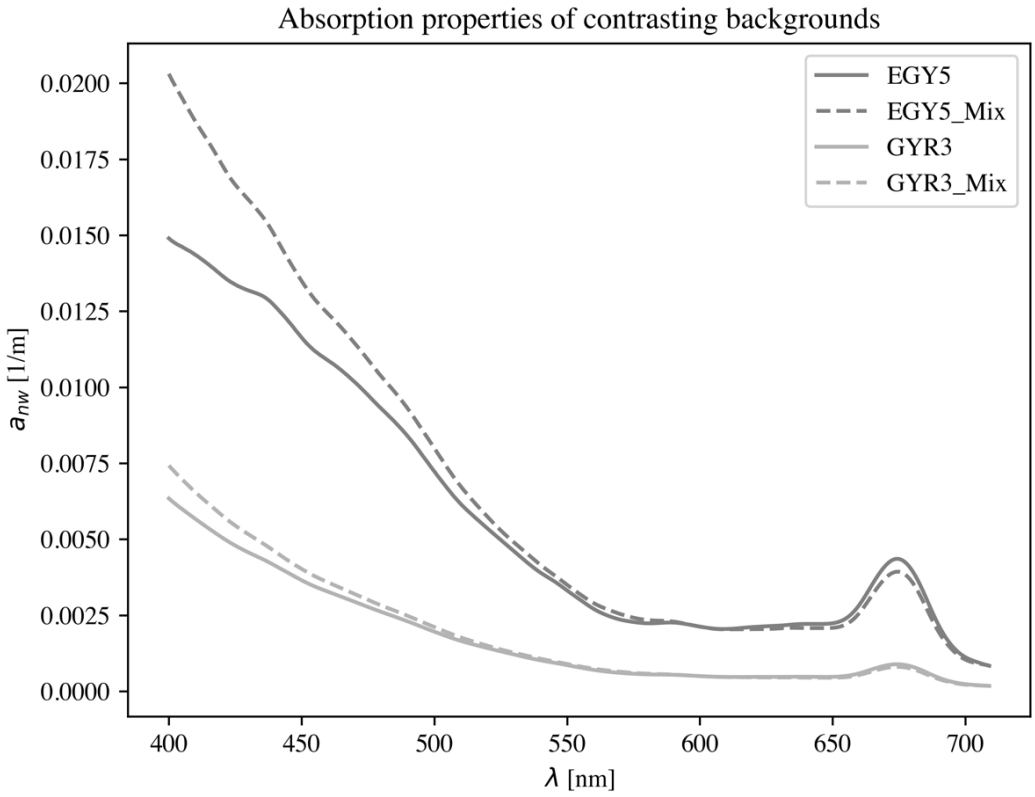

Figure S3. Absorption properties of dissolved and suspended material representing different backgrounds used in remote sensing reflectance simulations. The solid lines refer to the background material which approximated the GYR3 and EGY5 stations from the BIOSOPE cruise [6], while the dashed lines refer to the absorption properties of the mixture of VF17 and VF18 typical of natural variability in optical properties. Note that simulations with added microplastic were only prepared for the GYR3 and EGY5 backgrounds.

Microplastics

Simulations were performed for 10 microplastic concentrations added to the background material. The microplastic concentrations were 10 logarithmic steps between 1 and 200 mg m^{-3}. The microplastic content was composed of equal parts PEF2, PETG1 and PP1, which represent some of the most commonly found oceanic plastic debris [11]. These concentrations were used to scale the spectral mass-specific absorption and scattering coefficients. Microplastics were assumed to be homogenously distributed throughout the entire water column and mixed linearly with the background material.

To examine the detectability of microplastics at the top-of-atmosphere (ToA), we computed the upwelling radiance through multiplication of the R_{rs} by the solar constant binned to approximate bandwidths of the Sentinel-3 OLCI (10 nm). The resulting absolute change in L_w relative to the background L_w (i.e., ΔL_w) from added microplastics was compared with the technical specifications of the signal-to-noise ratio (SNR) for OLCI [12] and ΔL_w of the mixture of VF17 and VF18 background from the background using only VF18. We only consider microplastics detectable if ΔL_w of added microplastics exceeds both the SNR and the change in background deriving from varying background composition.

References

[1] Stamnes, K., Hamre, B., Stamnes, S., Chen, N., Fan, Y., Li, W., Lin, Z., & Stamnes, S. (2018) Progress in forward-inverse modeling based on radiative transfer tools for coupled atmosphere-snow/ice-ocean systems: A review and description of the AccuRT model. *Applied Sciences*, 8(12):2682. https://doi.org/10.3390/app8122682

[2] boergeh. (2024). boergeh/Flick-RT: Radiative transfer modeling framework (v1.0). *Zenodo*. https://doi.org/10.5281/zenodo.10551539

[3] Hu, Y. X., Wielicki, B., Lin, B., Gibson, G., Tsay, S. C., Stamnes, K., & Wong, T. (2000). δ-Fit: A fast and accurate treatment of particle scattering phase functions with weighted singular-value decomposition least-squares fitting. *Journal of Quantitative Spectroscopy and Radiative Transfer*, 65(4), 681-690. https://doi.org/10.1016/S0022-4073(99)00147-8

[4] Villevalde, & Smirnov, Alexander & O'Neill, & Smyshlyaev, Sergei & Yakovlev,. (1994). Measurement of aerosol optical depth in the Pacific Ocean and the North Atlantic. *Journal of Geophysical Research*. 99. 20983. https://doi.org/10.1029/94JD01618

[5] Koestner, D., Stramski, D., & Reynolds, R. A. (2020). Assessing the effects of particle size and composition on light scattering through measurements of size-fractionated seawater samples. *Limnology and Oceanography*, 65(1), 173-190. https://doi.org/10.1002/lno.11259

[6] Stramski, D., Reynolds, R. A., Babin, M., Kaczmarek, S., Lewis, M. R., Röttgers, R., Sciandra, A., Stramska, M., Twardowski, M. S., Franz, B. A., & Claustre, H. (2008). Relationships between the surface concentration of particulate organic carbon and optical properties in the eastern South Pacific and eastern Atlantic Oceans, *Biogeosciences*, 5, 171–201. https://doi.org/10.5194/bg-5-171-2008

[7] Bricaud, A., M. Babin, H. Claustre, J. Ras, & F. Tièche (2010), Light absorption properties and absorption budget of Southeast Pacific waters, J. Geophys. Res., 115, C08009. https://doi.org/10.1029/2009JC005517

[8] Stamnes, K., Hamre, B., Stamnes, J. J., Ryzhikov, G., Biryulina, M., Mahoney, R., Hauss, B., & Sei, A. (2011). Modeling of radiation transport in coupled atmosphere-snow-ice-ocean systems. *Journal of Quantitative Spectroscopy and Radiative Transfer*, *112*(4), 714-726. https://doi.org/10.1016/j.jqsrt.2010.06.006

[9] Gordon, H. R. (1999). Contribution of Raman scattering to water-leaving radiance: a reexamination. Applied Optics, 38(15), 3166-3174. https://doi.org/10.1364/AO.38.003166

[10] Morel, A., & Gentili, B. (2004). Radiation transport within oceanic (case 1) water. Journal of Geophysical Research: Oceans, 109(C6). https://doi.org/10.1029/2003JC002259

[11] Lebreton, L., Slat, B., Ferrari, F. et al. (2018). Evidence that the Great Pacific Garbage Patch is rapidly accumulating plastic. *Sci. Rep.* 8, 4666. https://doi.org/10.1038/s41598-018-22939-w.

[12] Donlon, C., Berruti, B., Buongiorno, A., et al. (2012). The global monitoring for environment and security (GMES) sentinel-3 mission. *Remote sensing of Environment*, *120*, 37-57. https://doi.org/10.1016/j.rse.2011.07.024